Pergamon

Acta mater. 48 (2000) 3895–3904

Acta MATERIALIA

www.elsevier.com/locate/actamat

SYNTHESIS OF POROUS Ni–Ti SHAPE-MEMORY ALLOYS BY SELF-PROPAGATING HIGH-TEMPERATURE SYNTHESIS: REACTION MECHANISM AND ANISOTROPY IN PORE STRUCTURE

B. Y. LI[1]*, L. J. RONG[1], Y. Y. LI[1] and V. E. GJUNTER[2]

[1]Institute of Metal Research, Chinese Academy of Sciences, Shenyang 110015, People's Republic of China and [2]Institute of Medical Materials and Shape Memory Implants, Tomsk 634034, Russia

(Received 25 February 2000; received in revised form 13 June 2000; accepted 13 June 2000)

Abstract—Porous Ni–Ti shape-memory alloys (SMAs) have attracted a great deal of attention recently because they have a similar microstructure to human bone and have significant prospects in medical applications. In the present study, equiatomic porous Ni–Ti SMAs, especially those with an unusual kind of linear-aligned elongated pore structure, have been successfully prepared by self-propagating high-temperature synthesis (SHS) using elemental nickel and titanium powders. The porous Ni–Ti SMAs thus obtained have an open porous structure with about 60 vol.% porosity, and the channel size is about 400 μm. The corresponding microstructural characteristics and the effect of preheating temperature on the microstructure have been investigated. It is found that the combustion temperature increases with increasing preheating temperature and results in melting of the NiTi compound above 450°C. Moreover, the preheating temperature has been shown to have a significant effect on the microstructure of the SHS-synthesized porous Ni–Ti SMAs, and the mechanism of anisotropy in pore structure is attributed to the convective flows of liquid and argon during combustion.

Keywords: Self-propagating high-temperature synthesis (SHS); Porous Ni–Ti; shape-memory alloys

1. INTRODUCTION

Metals and alloys are probably the most common materials used as surgical implants for artificial hard-tissue replacements. The biomaterials industry worldwide has an annual turnover of $2.3 billion in the field of hard-tissue repair and replacement (total of $12 billion). There has been and will continue to be a growing need for such biomaterials. However, common biomaterials can result in various problems usually related to the mismatch between the implant and the replaced bone. An implant is rejected when, regardless of its physicochemical and mechanical properties, it is not in good and permanent contact with body tissues. This seemingly simple task often cannot be resolved satisfactorily with the help of screws, glues, cements and/or plastics, or some intricate mechanical systems, but can be resolved successfully by using porous plates made of Ni–Ti shape-memory alloys (SMAs), which have a structure similar to that of sponge bone [1]. The biocompatibility of Ni–Ti is comparable to that of 316L stainless steel, as the presence of an adherent TiO_2 surface oxide can prevent nickel dissolution and release [2, 3]. Moreover, Ni–Ti SMAs have an attractive combination of properties such as excellent mechanical properties, good corrosion resistance and special shape-memory effect. In the applications of porous Ni–Ti SMAs as implants, their pores facilitate bone ingress and biological integration of the components, thus ensuring a harmonious bond between the implants and the body. It is interesting to note that studies of the physicomechanical properties of body tissues, including bones, under tensile loads have proved that living tissues have a high recoverable strain (> 2%) [1], showing a good "resilience", and only the pseudoelasticity of SMAs can exhibit similar deformation behavior. In addition, the Young's modulus of porous Ni–Ti SMAs can be easily adjusted to match that of the replaced bones because it can be controlled within a wide range via the choice of the porosity. Therefore, porous Ni–Ti SMAs are desirable for the treatment of congenital dislocation of the hip or pseudotalocrural articulation, and the replacement of bone and soft tissues in traumatology, dental surgery, otolaryngology and urology.

As mentioned before, the potential medical applications of porous Ni–Ti SMAs are considerable, but

* To whom all correspondence should be addressed.

1359-6454/00/$20.00
PII: S1359-6454(00)00184-1

realization of this requires new and innovative methods of preparation and design. Compared with traditional methods, self-propagating high-temperature synthesis (SHS) has the advantages of time and energy savings, and is being studied extensively for the fabrication of ceramic and intermetallic compounds [4, 5]. Most reports about the preparation of Ni–Ti SMAs by SHS [6–9] focus on obtaining dense Ni–Ti SMAs, and less attention has been paid on the preparation of porous Ni–Ti ones. In the present study, the porous feature of SHS products was purposely used to synthesize porous Ni–Ti SMAs.

It is important to select suitable powders and process parameters prior to SHS in order to prepare high-quality products, as the microstructure and properties of the final products depend on the SHS reaction conditions [10]. For example, in several intermetallic-forming SHS systems (Ni–Ti, Ni–Al, Ti–Si), the initial reactant powder mixture needs to be preheated, within a furnace, to even initiate the SHS reaction and form the desired intermetallic. Therefore, the effect of various processing parameters, such as reactant particle size of titanium and preheating temperature of the reactant, on the final microstructure was investigated.

Moreover, man-made porous materials tend to be almost isotropic [11], and properties are closely associated with microstructure. But a single piece of bone or cork differs in strength and stiffness by a factor of 2 or more along the two directions at right angles due to the anisotropic microstructure. Wood is more anisotropic still: some species of woods are 50 times stiffer when loaded along the grain than when loaded across it [12]. So we cannot ignore the directionality of pore structures; and it is a feature that can be built into man-made porous materials and exploited in engineering design. In fact, the potential for designing anisotropy into pore structure and exploiting it is considerable. However, less attention has been directed at understanding anisotropic porous materials. Therefore, another main aim of this study was to try to obtain porous Ni–Ti SMAs with anisotropic microstructure, mimicking the pore structure of wood and bones.

2. THERMODYNAMIC CONSIDERATIONS AND CALCULATION OF T_{AD}

2.1. Adiabatic combustion temperature, T_{ad}

Thermodynamic calculations can predict the ability to ignite or initiate a certain combustion reaction and help to optimize the preheating temperature as judged from reaction enthalpies. In order for a reaction to be self-sustaining it must be highly exothermic and therefore be associated with high temperatures. A key parameter that provides an indication of the temperature attained by the product during the reaction is the adiabatic combustion temperature, T_{ad}, defined as the temperature at which the enthalpies of the products are equal to those of the reactants at an initiation temperature T_p. This assumes that the enthalpy of the reaction heats up the products and that no heat energy is lost to the surrounding environment.

2.2. Calculation of T_{ad}

Consider the reaction between nickel and titanium to produce the intermetallic compound NiTi,

$$\mathrm{Ni} + \mathrm{Ti} = \mathrm{NiTi}. \tag{1}$$

The reaction occurs at an initiation temperature T_p. Since T_p is almost equal to T_0 in the present study, then the heat released during the reaction will be:

$$\Delta H^0 = \Delta H_f^0(T_0) + \int_{T_0}^{T_{ad}} C_p(p)\, dT, \tag{2}$$

where $\Delta H_f^0(T_0)$ is the enthalpy of formation of the intermetallic compound NiTi at temperature T_0, $C_p(p)$ is the heat capacity of the product and T_{ad} is the adiabatic combustion temperature. The rapidity of reaction (1) makes it reasonable to assume that the combustion reaction is pseudo-adiabatic, i.e., $\Delta H^0 = 0$. Hence, equation (2) becomes

$$-\Delta H_f^0(T_0) = \int_{T_0}^{T_{ad}} C_{p_s}(p)\, dT, \quad \text{if } T_{ad} < T_m \tag{3}$$

where T_m is the melting point of compound NiTi. If melting of the NiTi product occurs during combustion, then

$$-\Delta H_f^0(T_0) = \int_{T_0}^{T_m} Cp_s(p)\, dT + \nu \Delta H_m \quad (0 \le \nu \le 1), \quad \text{if } T_{ad} = T_m \tag{4}$$

and

$$-\Delta H_f^0(T_0) = \int_{T_0}^{T_m} C_{p_s}(p)\, dT + \Delta H_m + \int_{T_m}^{T_{ad}} C_{p_l}(p)\, dT, \quad \text{if } T_{ad} > T_m \tag{5}$$

where ΔH_m is the heat of fusion of the NiTi alloy, ν is the melting fraction of NiTi, and $C_{p_s}(p)$ and $C_{p_l}(p)$ are its heat capacities in the solid and liquid phases, respectively.

On the other hand, $\Delta H_f^0(T_0)$ can be calculated from

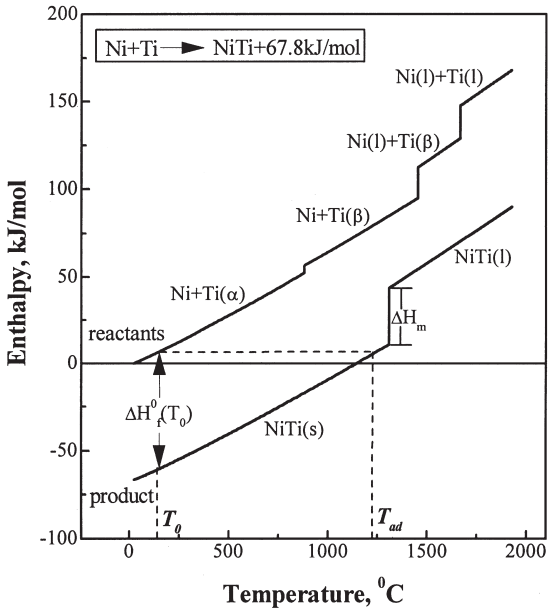

Fig. 1. The enthalpy–temperature diagram for the Ni/Ti system.

$$\Delta H^0_f(T_0) = \Delta H^0_{f,298} + \int_{298}^{T_0} \{C_p(\mathrm{NiTi}) - [C_p(\mathrm{Ti}) + C_p(\mathrm{Ni})]\}\, dT, \quad (6)$$

where $\Delta H^0_{f,298}$ is the heat of formation of compound NiTi at 25°C and C_p(Ti) and C_p(Ni) are the heat capacities of Ti and Ni, respectively.

Therefore, the adiabatic combustion temperature T_{ad} at a certain preheating temperature can be calculated by the above equation (3), (4) or (5). A schematic representation of this process is shown in Fig. 1, in which the thermodynamic data are taken from [9, 13].

3. EXPERIMENTAL

Table 1 presents the characteristics of the titanium and nickel powders used in this investigation. The powders were mixed according to the equiatomic Ni/Ti composition and tumbled for 24 h to ensure a homogeneous mixture. They were then pressed into cylindrical pellets with porosity around 58 vol.%. A hole was drilled at one end to accommodate the Pt/Pt–13% Rh thermocouple, which was used to record the temperature–time profiles. Each combustion reaction was conducted under an atmosphere of argon.

The general porosity of the specimens was calculated by the formula

$$\varepsilon = \left(1 - \frac{\rho}{\rho_0}\right) \times 100,$$

in which ρ and ρ_0 are the density of the specimen and its corresponding theoretical density, respectively. The density of the specimen was determined from its weight and dimensional measurements. The theoretical density is 6.19 g cm^{-3} (based on the values of pure Ni and pure Ti for equiatomic Ni–Ti powders) for the blended powders and 6.44 g cm^{-3} for the NiTi alloy. The general porosity consists of two parts, open porosity and closed porosity. The open porosity was determined by the liquid weighing method [14], and the open-porosity ratio is defined as the ratio of the open porosity to the general porosity. The channel size was determined using the method for chord analysis in the literature [15]; i.e., the pores interconnect into "channels" and the channel size was the average length of intersection of a random test line, which is perpendicular to the propagating wave direction, with the channels.

After reaction, X-ray diffraction (XRD), optical metallography and scanning electron microscopy (SEM) were performed on the specimens along the propagating wave direction and crosswise for analysis of the microstructural characteristics.

4. RESULTS

4.1. Microstructure evolution

4.1.1. XRD Fig. 2(a) shows an XRD pattern for the reactants. As can be seen, the nickel and titanium powders have been only mechanically mixed and no alloying has occurred. XRD patterns of SHS-synthesized porous Ni–Ti SMAs under different preheating temperatures are shown in Fig. 2(b). It can be found that the SHS process results in the formation of several intermetallic compounds, such as NiTi, Ti_2Ni, Ni_3Ti and Ni_4Ti_3, and no reflections corresponding to either of the reactants are observed. The B2(NiTi) and B19′(NiTi) phases, which are the desired products, are predominantly present.

4.1.2. Porosity, open-porosity ratio and channel size Table 2 presents the general porosity, open

Table 1. Powder characteristics of titanium and nickel

	Ti	Ti	Ti	Ni
Powder size (μm)	15.2	36.5	67.2	18.0
Specific surface area (m^2/g)	0.1976	0.0731	0.0434	0.0565
[O] (wt.%)	1.04	0.71	0.48	0.16

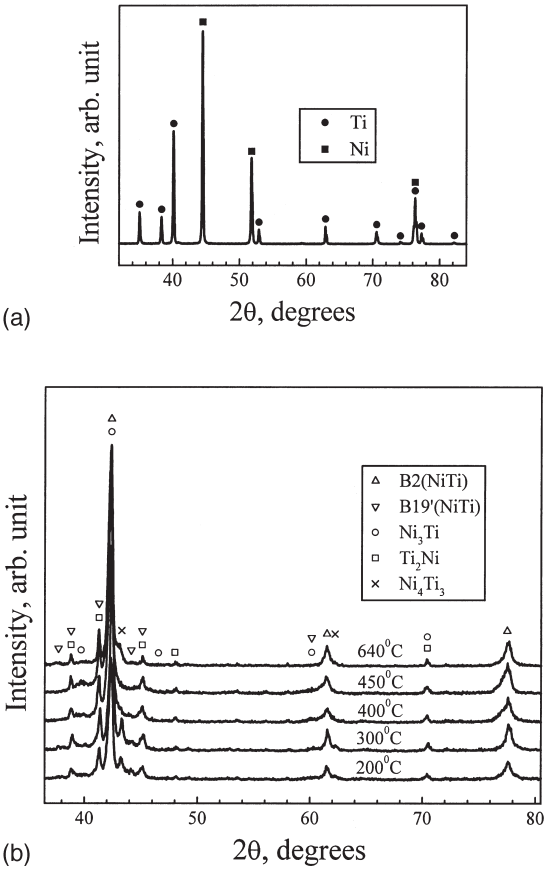

Fig. 2. XRD results for (a) the powder mixture and (b) SHS-synthesized porous Ni–Ti SMAs.

porosity, open-porosity ratio and channel size of the SHS-synthesized porous Ni–Ti SMAs. The general porosity of porous Ni–Ti SMAs is more than 60 vol.% and the open-porosity ratio is in excess of 0.85, which indicates that most pores interconnect into "channels". The corresponding channel size, about 400 μm, increases with increasing preheating temperature. It should be pointed out that the synthesized materials have great prospects in medical applications because, for implant materials with porosity in the range of 30–90%, the optimal channel size for bone tissue ingress is 100–500 μm [7].

4.1.3. Pore morphology and pore distribution Fig. 3 presents optical and SEM micrographs of porous Ni–Ti SMAs produced by SHS. One can see that the distribution of pores is uniform in the cross-section and that the pores are highly interconnected. There are also many isolated small pores interspersed in the matrix, and these pores are nearly spherical, which is obviously the result of transient liquid phase. Comparing the pore shapes in Fig. 3(c) and (d), evidence of microstructural inhomogeneity is observed at a preheating temperature of 300°C in the propagating wave direction, i.e., the longitudinal section. The pore shape is anisotropic: the pores are elongated in the direction of the propagating wave.

Fig. 4(a) shows macrographs of synthesized products. As can be seen, anisotropy of pore distribution can be found in the specimens with preheating temperature above 300°C, and the pores tend to be linear-aligned along the propagating wave direction with increasing preheating temperature. This pore orientation is different from that of porous materials produced by gas–eutectic transformation (GASAR) [16]. Fig. 4(b) shows the end of the as-synthesized products, in which obvious melting occurs. This demonstrates that a transient liquid phase once really existed during combustion and that the liquid quantity must increase with increasing preheating temperature. The corresponding cross-section of the products [Fig. 4(c)] shows that melting is serious and big pores form in the center of the products at preheating temperature above 450°C. In particular, a very large hole appears in the whole center of the product synthesized at a preheating temperature of 640°C.

The anisotropy in pore structure can also be found from Fig. 5, in which the longitudinal section of products synthesized at preheating temperatures of 300 and 400°C are shown. One can see "channels", which like the sap channels of a tree, are distributed along the propagating wave direction, and the channel size increases greatly with increasing preheating temperature. It can also be found that the "channel" distribution in the longitudinal section is very different from that in the cross-section [comparing Fig. 5(a) with 5(b)]. The channels are tortuous and almost completely interconnected in the cross-section, while the channels in the longitudinal section seem linear, parallel and less interwoven.

Table 2. The general porosity, open porosity, open-porosity ratio and channel size of porous Ni–Ti SMAs produced from Ti(15.2 μm) + Ni(18.0 μm)

	Preheating temperature (°C)				
	200	300	400	450	640
General porosity (%)	60.3	60.0	63.9	63.3	63.1
Open porosity (%)	55.8	54.2	54.7	–	–
Open-porosity ratio	0.925	0.904	0.856	–	–
Channel size (μm)	390	410	510	–	–

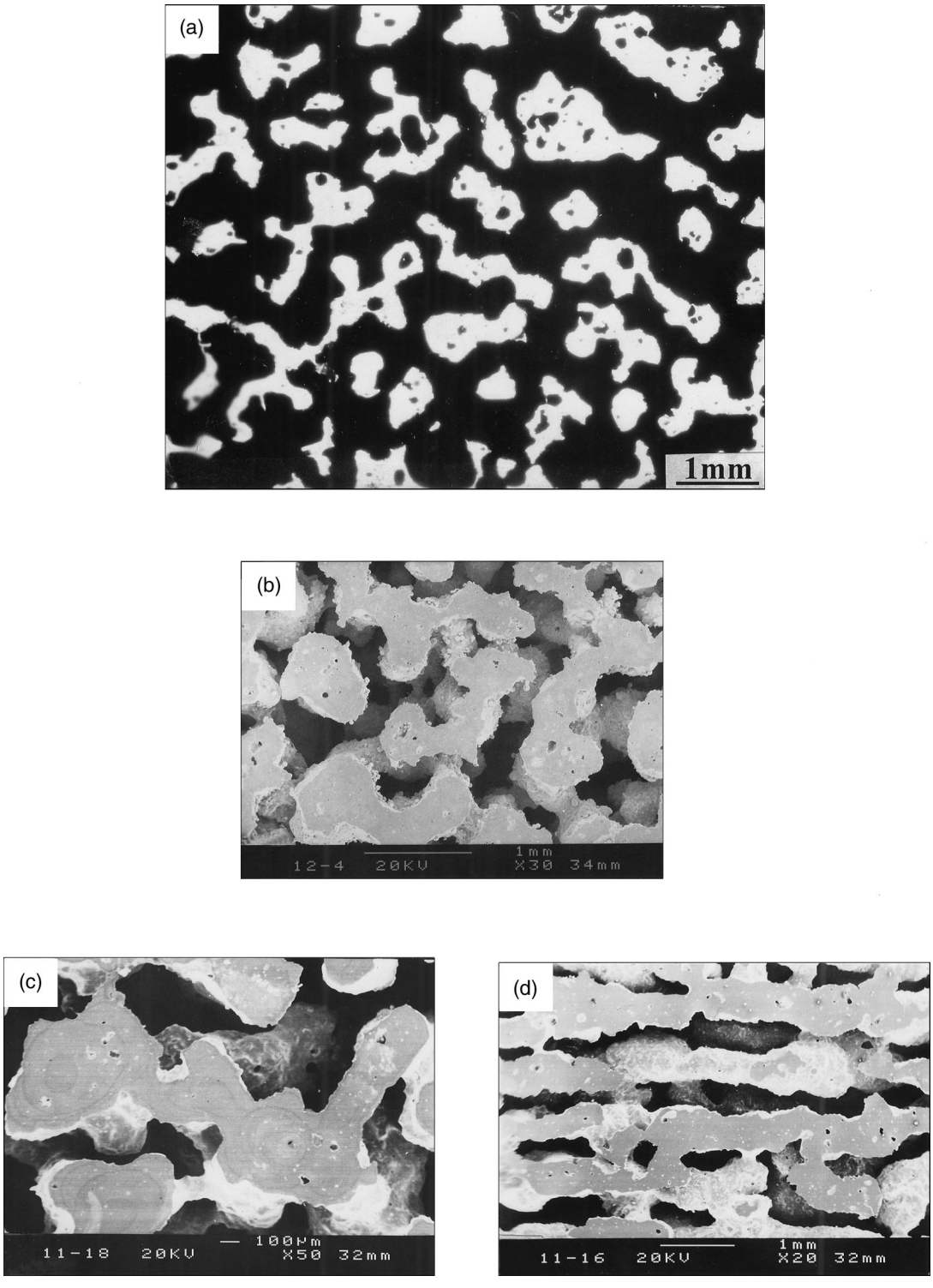

Fig. 3. Micrographs of porous Ni–Ti SMAs produced at different preheating temperatures. Cross-section: (a) optical micrograph, 200°C; (b) SEM, 200°C; (c) SEM, 300°C; longitudinal section: (d) SEM, 300°C.

4.2. Temperature–time profiles

The temperature–time profiles as indicated in Fig. 6 were obtained by placing a thermocouple at the center-line of the compact during the combustion wave propagation. When the combustion wave approaches the thermocouple, the curve indicates a very small increase in temperature of just several degrees from T_0 to T_p and, once the exothermic reaction propagates near to the location of the thermocouple, an abrupt rise in temperature is noticed. After that, the sample cools down as indicated by the decrease in temperature with increasing time.

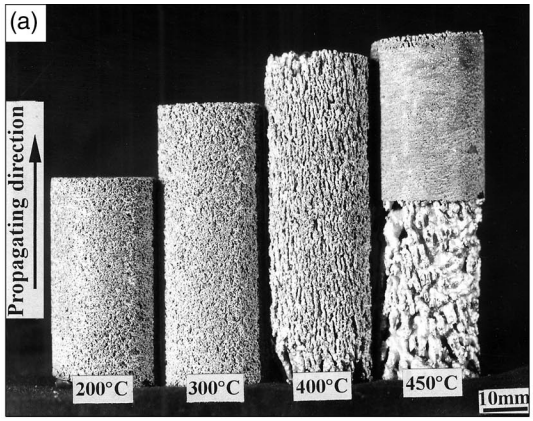

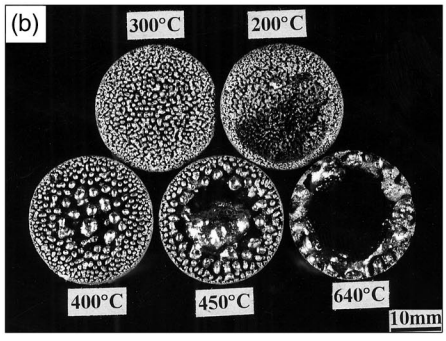

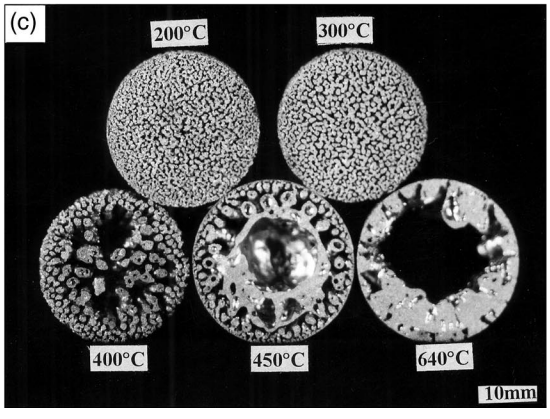

Fig. 4. Macrographs of porous Ni–Ti synthesized at different preheating temperatures. The propagating direction of the combustion wave is shown in (a). (a) Whole product; (b) the end of the as-synthesized product; (c) cross-section.

4.2.1. Influence of preheating temperature on the SHS process of porous Ni–Ti SMAs On account of the weak exothermic heat and low combustion temperature of the Ni + Ti reaction, combustion can only be initiated by preheating the compacts. It is found experimentally that when the preheating temperature of the powder compact is raised to or above 200°C, the combustion front is able to propagate. The temperature–time profiles with different preheating temperatures are shown in Fig. 6. Here, it can be seen that the combustion temperature, T_c, increases with increasing preheating temperature and reaches 1262°C at a preheating temperature of 450°C. Subsequently the combustion temperature changes little between preheating temperatures of 450°C and 640°C, and the measured combustion temperature of about 1260°C agrees well with the calculated adiabatic combustion temperature of 1310°C, i.e., the melting point of compound NiTi. This indicates that melting of NiTi occurs at preheating temperatures above 450°C. Also, it should be noted that the combustion does not propagate at a preheating temperature of 150°C while it propagates when the reactant is subsequently heated to 350°C [see Fig. 6(b)].

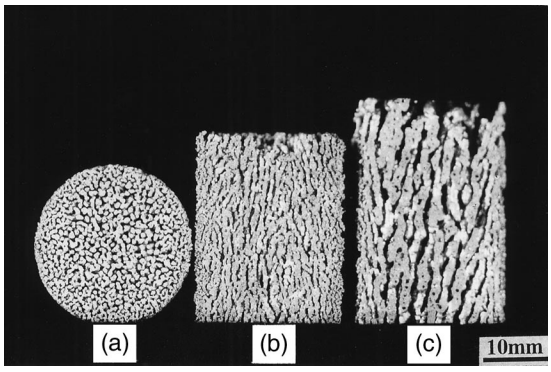

Fig. 5. Linear-aligned elongated pores in (a) the cross-section, (b, c) longitudinal sections of porous Ni-Ti SMAs synthesized at a preheating temperature of 300°C (a, b) and 400°C (c).

4.2.2. Influence of particle size of Ti on the SHS process of porous Ni–Ti SMAs The influence of reactant particle size of Ti on the combustion temperature is presented in Fig. 7. It is found that the particle size of Ti has a complex effect on the combustion process. At the same preheating temperature, Ti(15.2 μm) + Ni(18.0 μm) and Ti(67.2 μm) + Ni(18.0 μm) have high combustion temperatures and the difference between their combustion temperatures is small. On the other hand, Ti(36.5 μm) + Ni(18.0 μm) has a much lower combustion temperature.

4.3. Calculation results of T_{ad} and comparison with experimental data

From Fig. 6, it is found experimentally that $T_p \approx T_0$. Therefore, the influence of preheating temperature T_0 on adiabatic combustion temperature T_{ad} calculated according equations (3), (4) and (5) is shown in Fig. 8 assuming that $T_p \approx T_0$. As can be seen, T_{ad} increases almost linearly with increasing T_0 below 227°C, followed by a plateau between 227 and 750°C. Finally, T_{ad} increases again with further increases in T_0. At preheating temperatures between 227 and 750°C, T_{ad} reaches the melting temperature of NiTi, and the melting fraction increases almost linearly with increasing T_0. Complete melting occurs at T_0 of 750°C as can be seen in the inset.

Although SHS reactions can be generally characterized by the adiabatic combustion temperature, it must be remembered that loss of heat to the surround-

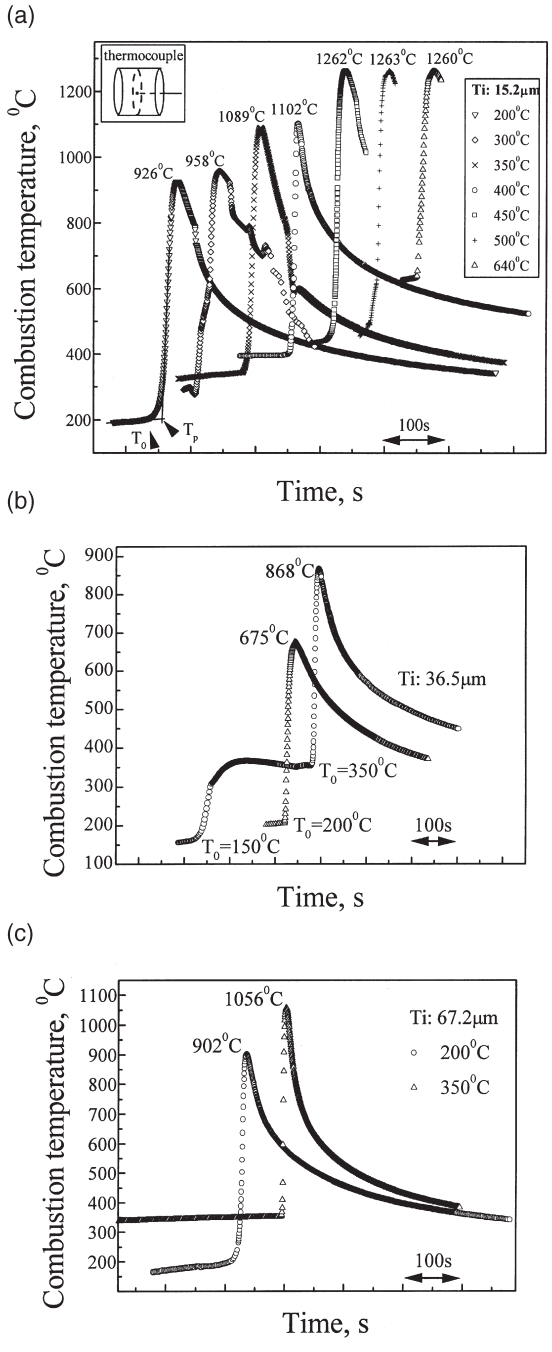

Fig. 6. The influence of preheating temperature on combustion temperature during SHS of porous Ni–Ti SMAs. As shown in (a), $T_p \approx T_0$. (a) Ti(15.2 μm) + Ni(18.0 μm); (b) Ti(36.5 μm) + Ni(18.0 μm); (c) Ti(67.2 μm) + Ni(18.0 μm).

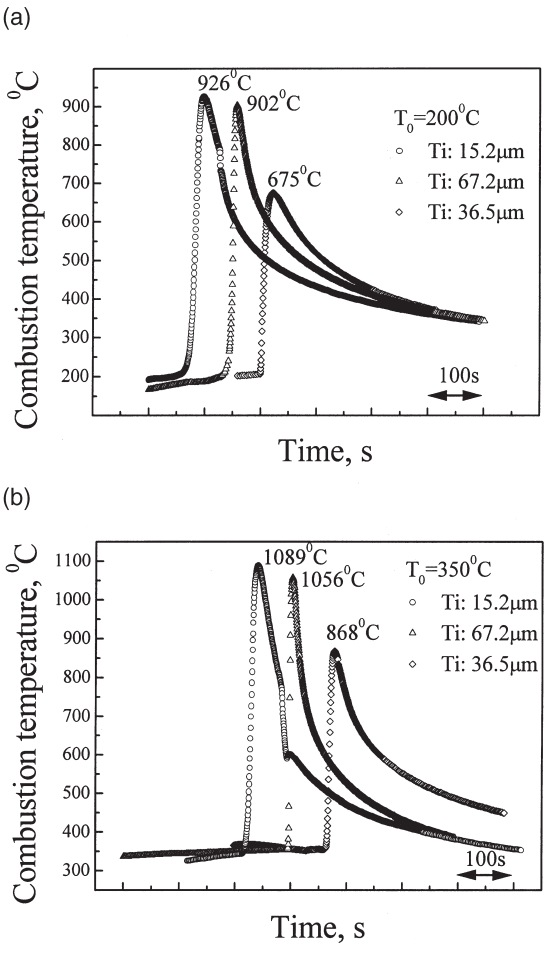

Fig. 7. The influence of particle size of Ti on combustion temperature during SHS of porous Ni–Ti SMAs at preheating temperatures of (a) 200°C and (b) 350°C.

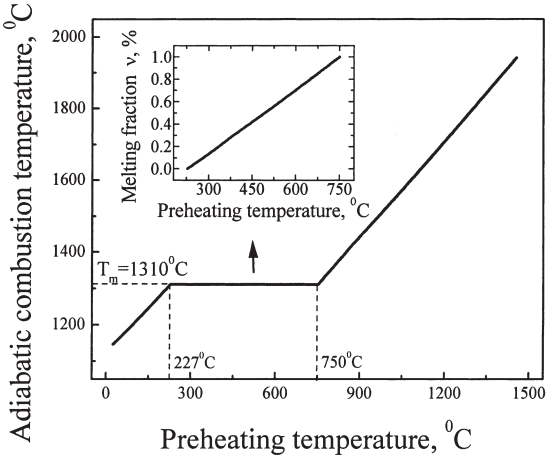

Fig. 8. Graph of calculated adiabatic combustion temperature versus preheating temperature.

ings is unavoidable and sometimes can be significant, especially with samples of high surface area/volume ratio [17, 18]. The experimental measurements of T_c are shown in Fig. 9, in which the calculated adiabatic combustion temperature is also shown for comparison. As can be seen, T_c is lower than the corresponding T_{ad}, and the lower T_0 the greater the variation between T_{ad} and T_c.

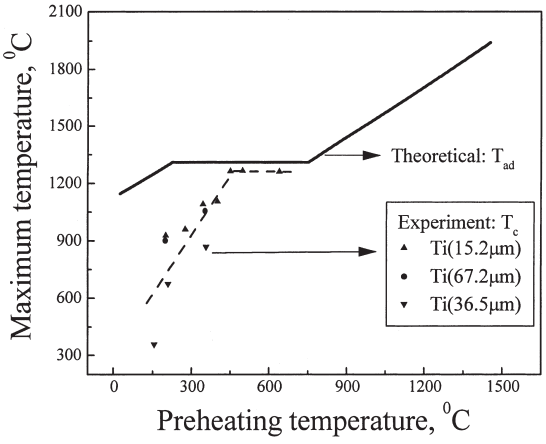

Fig. 9. Graph of combustion temperature and calculated adiabatic combustion temperature versus preheating temperature.

5. DISCUSSION

Fig. 10 shows the Ni–Ti binary diagram [19]. The system is characterized by three stable intermetallic compounds. Of particular interest in this study is NiTi, although metastable intermetallics such as Ni_4Ti_3 and $Ni_{11}Ti_{14}$ can also sometimes be observed [20]. In the present study, a stoichiometric mixture of nickel and titanium powders is used to form an intermetallic compound product NiTi. The reactions between nickel and titanium are initiated and heat, which further accelerates the reaction and makes it self-sustaining, is liberated because of the thermodynamic stability of the intermetallic compounds. NiTi is the dominant phase due to the equiatomic Ni/Ti composition, while Ti_2Ni, Ni_3Ti and Ni_4Ti_3 can also be observed. The appearance of second phases, which is a common feature for all samples produced by SHS [21], can be explained by the characteristics of SHS. The elemental reactant powders are not mixed sufficiently well and/or the particle size of the reactants is insufficiently small, and as a result there is a composition fluctuation in the specimen that is responsible for the formation of different second phases during SHS.

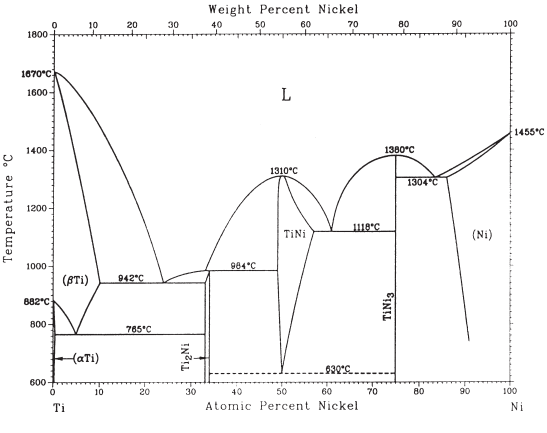

Fig. 10. The Ni–Ti phase diagram.

Fig. 3, showing the micrographs of porous Ni–Ti SMAs produced by SHS, demonstrates the porous nature of the SHS reaction products. As pointed out by Munir and Wang [22], pores in SHS-reacted products have five possible sources. They are: (1) existing pores in the reactants prior to combustion; (2) differences in molar volume between reactants and products; (3) differences in diffusion rates between nickel and titanium; (4) gas evolution during reaction; and (5) thermal migration due to the high temperature gradient during combustion. Certainly, the first one is the main contribution since the reactants prior to combustion have porosity about 58 vol.%. It is also believed that the last two contributions are important in this work.

From equations (3), (4) and (5), it is found thermodynamically that a higher preheating temperature results in a higher adiabatic combustion temperature and thereby a higher combustion temperature T_c. Judged from Fig. 6(a) or Fig. 9, it can be found that NiTi melts at $T_c \approx 1260$°C, which is lower than the melting point of NiTi indicated in the phase diagram (Fig. 10). The reason for the discrepancy between the measured T_c (about 1260°C) and the melting point of NiTi (1310°C) can be explained as follows: (1) the combustion temperature measured by the thermocouple may be lower than the actual combustion temperature in the specimen, because the combustion reaction rate is very fast and the combustion temperature gradient is very high during SHS while the response rate of the thermocouple is limited; and (2) the melting point of NiTi prepared by powder metallurgy may be a little lower than that produced by arc-melting. Moreover, the SHS process cannot be ideally adiabatic, thus heat loss due to heat flow from the reaction zone to the surroundings is unavoidable, and the combustion temperature is lower than the adiabatic combustion temperature. If the heat loss is too large and the heat provided by preheating is too low, then combustion may be quenched. This can be used to explain why SHS cannot propagate when the preheating temperature is at or below 150°C. It has been found that the particle size of Ni has little effect on combustion temperature during SHS of Ni–Ti SMAs [9]. However, the present study shows that the particle size of Ti has a complex effect on the combustion temperature. The reason is not very clear at present and further investigation is in progress.

The mechanism of SHS of porous Ni–Ti SMAs varies with the SHS processing conditions. When the maximum temperature that can be reached, i.e., T_c, is below the lowest eutectic temperature (942°C) in the Ni–Ti system (Fig. 10), no liquid possibly exists, and solid-state reaction is the dominant mechanism. The original pores in the compact and formed Kirkendall pores are the main pore origins of the final products. When T_c is above the lowest eutectic temperature yet at a temperature where the compound NiTi product is solid, a transient eutectic liquid corresponding to Ni–76 at.% Ti forms, rapidly wets and spreads

throughout the reaction front due to the capillary force. The liquid consumes the elemental powders and finally forms mainly NiTi products behind the advancing liquid interface. The presence of liquid enhances material transport and homogenization, thus diffusion and capillary action would all act as reaction mechanisms. When the preheating temperature is increased further, T_c can reach or exceed the melting point of NiTi and a relatively large quantity of liquid may exist. Then capillary spreading of the liquid will be the main mechanism and even a cast product may be obtained at high preheating temperature.

It is thought that the significant difference in the channel distribution of the present porous Ni–Ti SMAs is largely determined by the transient liquid during combustion. A combustion reaction is often associated with various kinds of fluid flow. For instance, if combustion is carried out under an inert or reactive gas atmosphere, convective flow of gas will occur due to a temperature gradient existing in the atmosphere when a combustion wave is initiated. Also, owing to the nature of the combustion reaction, a large temperature gradient exists within the liquid layer, which could induce flow of liquid phase within the combustion front. In the present reaction system, there are two kinds of fluid: (1) the eutectic liquid and/or molten matrix NiTi phase that are produced at the combustion front; and (2) argon gas, which is introduced to protect the ignition coil and sample. Fluid flow, especially convective liquid flow, enhances both the heat and mass transfer rates. It should be noted that the liquid flow is also impeded by the presence of the solid products. Thereby, once liquid forms, the pore structure will be affected by the advancing solid/liquid interface, depending on the quantity of the liquid, the convective argon flow and the temperature gradient. When the preheating temperature is relatively low, there is no liquid, or the quantity of liquid, which is entrapped by the interface, is small; as a result, no anisotropy in pore structure occurs. That is why no obvious microstructural anisotropy is observed when the reactants are preheated at 200°C. However, when the preheating temperature increases to a certain value (for example, 300°C), the quantity of liquid, which even forms continuously in the reaction front, increases, and the liquid persists for a little longer due to the higher combustion temperature. Meanwhile, a much higher temperature gradient exists between the product and the reactants. In these cases, although the thermal wave moves rapidly, the wetting liquid quickly encapsulates and consumes small pores and forms relatively large channels, which are sheared in the propagating direction by the conveyor motion of liquid and argon. The convective argon flow further accelerates the motion of the liquid flow. Therefore, anisotropy in pore structure appears and becomes serious with further increases in preheating temperature, and the channel size increases with increasing preheating temperature. When T_c reaches the melting point of the NiTi compound, a large part of the product is in the liquid phase and also there is a small temperature gradient between the center and the periphery of the specimen; thereby a big hole will form in the center throughout the product. It should be noted that the high temperatures encountered during the SHS reactions often result in the expulsion of any volatile impurities or moisture that may be found in the starting powders. Therefore, it is thought that the expulsion of impurity gases and the convective flow of argon and liquid all contribute to the high open-porosity ratio in the present study.

It has been observed that convective fluid flow can change the combustion behavior as well as the microstructure of the reacted products [23]. It can therefore be concluded that a liquid phase is important in inducing the anisotropy in microstructure of porous Ni–Ti SMAs. The mechanism of formation of anisotropy in pore structure at or above a preheating temperature of 300°C may be summarized as follows, based upon the experimental results observed. As the liquid/solid interface moves along the propagating direction, the pores grow, accompanying the flow of the liquid. If the quantity of liquid is small, then the liquid will be entrapped by the interface and no anisotropy of pore distribution will occur. However, when the quantity of liquid increases to a critical value, the liquid will flow along the propagating wave direction due to both gas flow and the high temperature gradient. Therefore, pores grow along the propagating wave direction and anisotropy of pore structure appears.

6. CONCLUSIONS

Porous Ni–Ti SMAs, especially those with a new kind of pore structure with linear-aligned elongated pores, have been successfully prepared by an SHS reaction of Ni and Ti powders. The porous Ni–Ti SMAs thus obtained have an open porous structure with about 60 vol.% porosity, and the channel size is about 400 μm. The effects on combustion temperature of reactant particle size of Ti and preheating temperature, which has been employed to increase the combustion temperature by increasing the adiabatic combustion temperature, have been investigated. Upon preheating the reactants the adiabatic combustion temperature can be increased to form a transient eutectic liquid and/or even to melt compound NiTi product. The microstructure of the product has been shown to be highly dependent on the preheating temperature. It is thought that the unusual pore structure with linear-aligned elongated pores observed with this particular reaction is closely associated with the liquid phase formed and the convective argon flow.

REFERENCES

1. Korotayev, A., Gjunter, V. and Itin, V., *Science in the USSR*, 1989, **2**, 60.

2. Green, S. M., Grant, D. M. and Kelly, N. R., *Powder Metall.*, 1997, **40**, 43.
3. Shabalovskaya, S., Cunnick, J., Anderegg, J., Harmon, B. and Sachdeva, R., in *Proceedings of 1st International Conference on Shape Memory and Superelastic Technologies, Asilomar, CA, March*. SMST Organising Committee, 1994, p. 209.
4. Merzhanov, A. G. and Khaikin, B. I., *Prog. Energy Combust. Sci.*, 1988, **14**, 1.
5. Dunmead, S. D., Readey, D. W., Semler, C. E. and Holt, J. B., *J. Am. Ceram. Soc.*, 1989, **72**, 2318.
6. Yi, H. C. and Moore, J. J., *Scripta metall.*, 1989, **22**, 1889.
7. Itin, V. I., Gjunter, V. E., Shabalovskaya, S. A. and Sachdeva, R. L. C., *Mater. Character.*, 1994, **32**, 179.
8. Otaguchi, M., Kaieda, Y., Oguro, N., Shite, S. and Oie, T., *J. Jpn Inst. Met.*, 1990, **54**, 214.
9. Yi, H. C. and Moore, J. J., *J. Mater. Sci.*, 1989, **24**, 3449.
10. Munir, Z. A. and Tamburini, U. A., *Mater. Sci. Rep.*, 1989, **3**, 278.
11. Ashby, M. F., *Metall. Trans.*, 1983, **14A**, 1755.
12. Gibson, L. J. and Ashby, M. F., in *Cellular Solids: Structure and Properties*. Cambridge University Press, Cambridge, UK, 1997, p. 389.
13. Barin, I., Knacke, O. and Kubaschewdki, O., in *Thermochemical Properties of Inorganic Substances*. Springer Verlag, 1977, Suppl..
14. *ASTM Standard B328*. American Society for Testing and Materials, Philadelphia, PA, 1987.
15. Smith, D. M., Hua, D. W. and Earl, W. L., *MRS Bull.*, 1994, (April), 44.
16. Simone, A. E. and Gibson, L. J., *Acta mater.*, 1996, **44**, 1437.
17. Bowen, C. R. and Derby, B., *British Ceram. Trans.*, 1997, **96**, 25.
18. Maksimov, E. I., Merzhanov, A. G. and Shkiro, V. M., *Combust. Explos. Shock Waves*, 1965, **1**, 15.
19. Massalski, T. B., Okamoto, H., Subramanian, P. R. and Kacprzak, L., in *Binary Alloy Phase Diagrams*. ASM International, 1996, p. 2874.
20. Busch, J. D., Berkson, M. H. and Johnson, A. D., *Proc. MRS Symp.*, 1991, **230**, 91.
21. Yi, H. C., Moore, J. J. and Petric, A., *Metall. Trans.*, 1992, **23A**, 59.
22. Munir, Z. A. and Wang, L. L., in *Proceedings of 1st US–Japanese Workshop on Combustion Synthesis*, eds Y. Kaieda and J. B. Holt, 1990, p. 123.
23. Yi, H. C., Woodger, T. C., Moore, J. J. and Guigne, J. Y., *Metall. Trans.*, 1998, **29B**, 889.